Available online at www.sciencedirect.com
ScienceDirect
International Journal of Solids and Structures 44 (2007) 3156–3176
INTERNATIONAL JOURNAL OF SOLIDS and STRUCTURES
www.elsevier.com/locate/ijsolstr

Linear coupled bending and extension of an unbalanced bonded repair

R.J. Clark *, D.P. Romilly

University of British Columbia, Department of Mechanical Engineering, 2054-6250 Applied Science Lane, Vancouver, BC, Canada V6T1Z4

Received 9 May 2006; received in revised form 18 July 2006
Available online 19 September 2006

Abstract

An unbalanced repair is a composite patch bonded to one side of a cracked structure for the purpose of preventing or reducing damage growth in the substrate. A single-sided repair offsets the load path within the structure, inducing out-of-plane bending. This bending increases the stress intensity in the underlying crack and causes adhesive peel stresses and bending of the repair which can, relative to a repair that is restrained against bending, lead to early failure. In this article the authors correct the analysis of Wang and Rose [Wang, C.H., Rose, L.R.F., 1997. On the design of bonded patches for one-sided repair. In: Proceedings of the 11th International Conference on Composite materials, Gold Coast, Australia, vol. 5, pp. 347–356] developed by using an energy analysis of a single-sided or unbalanced repair applied to a very long-crack, to comply with Maxwell's reciprocal theorem and to account for transverse normal and shear stresses at the crack tip and the accompanying shear deflections. The authors then develop closed-form equations useful for bonded composite repair design and damage tolerance assessment of cracks of arbitrary length by developing a new method for interpolation between this long-crack limit and a short-crack limit based on the stress intensity and crack face displacements for an unreinforced crack. The interpolation method is then tested against an advanced line-spring model that has been created by using a 6th order generalized plane strain plate formulation in extension and a new 8th order formulation in bending, thus allowing for the inclusion of transverse shear and normal stresses. The closed-form equations are found to be accurate when compared to the line-spring model, and to provide reasonable results when compared to a three-dimensional finite element model of a bonded repair. Inaccuracies are shown to exist principally in the determination of the nominal stresses in the vicinity of the crack.

Keywords: Bonded repair; Damage tolerance; Bending; Coupling; Line-spring; Fatigue; Fracture

1. Introduction

A bonded composite repair consists of a filamentary composite reinforcement that is bonded to a damaged or weakened structure to reduce stresses and prevent or reduce continuing damage growth. Such repairs are an

* Corresponding author. Tel.: +1 604 827 5821; fax: +1 604 822 2403.
E-mail address: clark.randal@gmail.com (R.J. Clark).

0020-7683/$ - see front matter © 2006 Elsevier Ltd. All rights reserved.
doi:10.1016/j.ijsolstr.2006.09.012

Nomenclature

a	half crack length
t	thickness or distance from centre of crack
u	crack face deflection
y	coordinate taken from centre of crack
z	coordinate taken from plate centre line
k	spring stiffness
c	spring compliance
D	plate bending constant, $Et^3/12$
G	strain energy release rate or shear modulus
K	stress intensity
E	Young's modulus
S	stiffness ratio, $E_r t_r/E_p t_p$
M	line moment, or moment per unit length acting on a cut in a plate
N	line force, or force per unit length acting on a cut in a plate
Y	geometry correction factor

Greek symbols

α	normalized crack length
θ	rotation
μ	shear modulus
v	Poisson's ratio
η	effective Poisson's ratio for transversally isotropic plate, $\eta = v^z\sqrt{E/E^z}$
σ	stress
κ	parameter arising from differential equations

Subscripts

p	plate
r	reinforcement
a	adhesive
m	membrane
b	bending

Superscripts

r	reinforced result from interpolation model
n	numerical result from line-spring model
0	nominal result without including crack bringing springs
∞	long-crack limit result including crack bringing springs
z	transverse property
pres.	correction for transverse pressurization
shear	correction for transverse shear

effective method by which to extend the life of aircraft structures, offering advantages in effectiveness, weight, profile, application time, cost, and inspectability when compared to mechanically fastened repairs. Bonded composite repairs have seen significant use in military applications but limited use in civil aviation, primarily due to certification issues. Repairs to primary or structurally significant aircraft structures are required to meet Damage Tolerance (DT) requirements, which are outlined in FAA Circular 25.571-1C (1998), effectively requiring an assessment of the residual life of the part and the development of an inspection schedule suitable for the detection of damage before the failure of the structure. Accordingly, models are required for the pre-

diction of the fatigue life and residual strength of repaired structures. In this article, the authors develop closed-form equations for the analysis of an unbalanced repair, where the patch is bonded to only one side of a cracked structure, and induces out-of-plane bending by offsetting the load path. Bending increases the stress intensity in the underlying crack and causes adhesive peel stresses and bending of the repair that, if not properly accounted for in the analysis, could lead to premature failure.

A significant body of work exists for the analysis of bonded composite repairs, which can be separated into two broad classes, balanced or double-sided repairs and unbalanced or single-sided repairs (Fig. 1). Closed-form equations useful for composite repair design and damage tolerance analysis have existed for some time for balanced repairs, in which patches are applied to both sides of a cracked plate or in which the repaired plate exhibits a large degree of bending restraint due to underlying structure. The most significant contributions have been from Rose (1981, 1982, 1988), who established an upper limit on the stress intensity for a very long reinforced crack by means of an energy analysis. By using this long-crack solution as an upper limit and the nominal, or unreinforced solution as a short-crack limit, Rose developed a very effective interpolation for cracks of arbitrary length. Wang and Rose (1998) have demonstrated that for extension of reinforced plates the long-crack limit needs to be modified to account for the plane strain conditions present at the crack tip. Clark and Romilly (submitted for publication-a) have developed a generalized plane strain line-spring model for plate extension and developed a set of geometry correction factors for finite thickness plates which allows for accurate determination of both the stress intensity and crack opening displacement in balanced repairs. The closed-form equations of Rose have been adapted to the analysis of repairs with finite planar dimensions via the inclusion analogy (Rose, 1981), with significant shear lag in the composite patch (Jones et al., 1983), for partially disbonded repairs (Baker, 1993,Clark and Romilly, 2001), and for tapered repairs (Albat and Romilly, 1999). These closed-form methods allow for simplified damage tolerance analysis, reliability assessment, and design optimisation of repairs.

There is much interest in the application of unbalanced repairs, as often only one face of a structure is exposed. Often the interior structure of the aircraft does not provide restraint against bending, and application of the repair will result in significant out-of plane loading due to a shift in the neutral axis. For balanced repairs, failure typically occurs by progressive cracking and adhesive disbonding. Composite fibre and matrix failures are rare except in the presence of compressive loading or bending induced by geometric details or lack of restraint. For unbalanced repairs, composite failure mechanisms such as inter-ply delamination and frac-

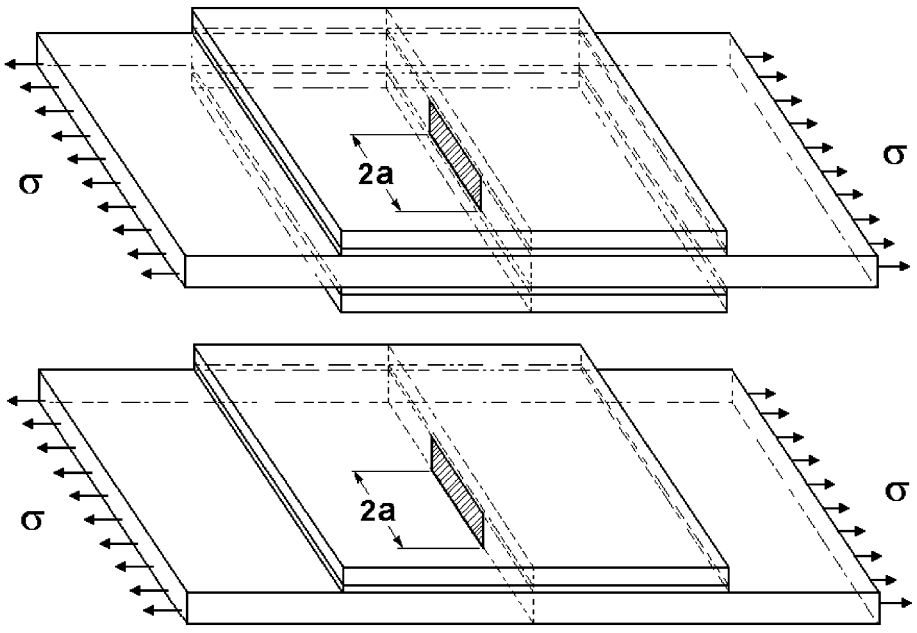

Fig. 1. Repair configurations: balanced (top) and unbalanced (bottom).

ture are more likely to occur in conjunction with cracking and disbonding. Jones et al. (1995) have reviewed the failure modes and damage locations observed in both laboratory and in-service military use of bonded repairs. They conclude that, besides substrate cracking and cohesive disbonding of the repair, damage tolerance assessment should include fibre failure, adhesive failure, cohesive failure at the patch-adhesive interface, adhesive failure at the adhesive-substrate interface, plus inter-laminar failure and delamination. These aspects are reflected in the FAA circular, which requires the assessment of the repaired structure, adhesive, and composite repair, including impact damage, inter-ply delamination, and adhesive disbonding. To streamline the design and certification of repairs, particularly single-sided repairs, closed-form methods are needed to assess the effects of bending on the rate of failure of the repaired structure, but perhaps more importantly, methods are required to assess the life and strength of the repair itself under bending and transverse normal (peel) stresses.

Many studies have been carried out in an effort to characterize the effect of bending. The first result is due to Ratwani (1979) who developed a bending correction factor by adding the bending stress expected in the outer fibre of the plate to the nominal stresses in the crack plane, allowing the results for a symmetric repair to be applied to a one-sided repair. Early finite element studies by Jones (1983), set out the framework by which two-dimensional finite element models of plates can be extended to the analysis of adhesively bonded layered plates. Several studies have focussed on producing numerical methods such as three-layer finite element analyses (Arendt and Sun, 1994; Schubbe and Mall, 1999), boundary element methods (e.g. Wen et al., 2002), or automated damage growth in fully three-dimensional models (e.g. Papanikos et al., 2005) in order to predict the life of a repaired structure. The focus of this article is the development of closed-form methods that are easily adaptable to damage tolerance or reliability analysis and design optimisation. As for the analysis of balanced repairs, Australian researchers have led the field in the development of closed-form methods. Rose (1988) developed a bending correction factor for the long-crack case that includes geometrically nonlinear (stress-stiffening) effects by considering the adhesive as providing a rigid bond and applying an energy analysis to determine the strain energy release rate for a very long-crack. More recently, Wang and Rose (1997) have developed an expression for the total strain energy release rate for a long-crack bridged by coupled bending and extensional springs, and a method for separation of this strain energy release rate into the membrane and bending stress intensity components. Unfortunately, by comparison to a three-dimensional finite element analysis, they concluded that their energy method significantly over-predicts the bending stress intensity and thus was not valid or useful for the design of a repair. Wang et al. (1998) went on to develop an analytical approach for separation of the strain energy release rate (expressed as the root-mean-square stress intensity) by assuming that the bending and membrane components act in the same ratio regardless of the length of the crack. By considering the short-crack limit, where the springs bridging the crack faces do not provide any constraint to the motion of the crack faces, the membrane and bending stress intensity components are linearly related to the membrane and bending stresses in the substrate in the plane of the crack, and this ratio could easily be determined. They continued by developing an interpolation between the long-and short-crack limit solutions for the root-mean-square stress intensity, allowing the membrane and bending stress intensity to be calculated for a crack of arbitrary length. Unfortunately, as this approach assumes that the membrane and bending stress intensities act in the same proportion for any crack length, the validity of the approach must be assessed on a case-by-case basis, particularly if it is to be extended to nonlinear analysis of a repair or to new repair geometries. This approach also provides no information regarding the stresses in the adhesive or the composite patch near the crack.

Through the work of Australian researchers (primarily Rose and Wang), closed-form equations exist that establish a conservative upper limit on the root-mean-square stress intensity at the crack tip. Unfortunately, the energy methods that have been very successful for the analysis of tensile loading of double-sided repairs, have otherwise been abandoned in favour of line-spring models for analyzing the case of coupled bending and extension (Rose and Wang, 2002). In a recent conference paper, Romilly and Clark (2005) stated that a corrected form of the energy method of Wang and Rose (1997), which establishes long-crack limits for the membrane and bending stress intensity in a repair, is in fact very accurate when compared to the predictions of generalized plane strain line-spring models which capture the three-dimensional behaviour of the plate near the crack tip. In this article, the authors continue by fully describing the line-spring model and using it to validate an interpolation approach that is valid for cracks of arbitrary length. This methodology and the resulting

analysis are then tested against a three-dimensional finite element model, demonstrating very accurate results for both the membrane and bending stress intensity and the crack face displacements, which may be related to the stresses in the adhesive and in the composite patch.

2. A methodology for patch damage tolerance assessment

In keeping with the two-step approach introduced by Rose (1981, 1982), several elements are required to complete the analysis of a bonded composite repair. The first step is to determine the stresses in the plane of the crack for the prospective repair. Due to load transfer from the plate to the patch, this stress will normally be reduced from the stress in the plate before application of the repair. The second step is to perform an analysis to determine the stress intensity and the stresses in the repair in the region of the crack. To achieve this, it is first necessary to characterize the stiffness of the repair as it acts to restrain the opening of the crack. Once these two steps are completed, a crack-bridging model is used to predict the stress intensity in the plate and the stresses in the adhesive and the composite repair. This is usually achieved by interpolation between limit states developed from an energy analysis of a very long-crack bridged by springs and a very short crack without reinforcement. The resulting interpolation solution is applicable to a crack of arbitrary length.

2.1. Stress in the crack plane

The work of Wang and Rose (1999) provides a set of useful expressions for the plate stresses in the vicinity of the crack. By their analysis one can consider that the shear and peel stresses in the adhesive bond joining the repair patch to the plate will vanish in areas remote from the edges of the repair, the plate and repair may be considered to be rigidly bonded, and that the membrane and bending stresses in the plate may be calculated by considering the structure to be a simple composite beam. The neutral axis of the combined structure is offset from the centreline of the repaired plate by a distance $\bar{z}$, calculated as follows:

$$\bar{z} = \frac{S(t_\mathrm{p} + t_\mathrm{r})}{2(1+S)} \tag{1}$$

The moment of inertia of the reinforced plate is then calculated from

$$I_t = \frac{t_\mathrm{p}^3}{12} + t_\mathrm{p}\bar{z}^2 + \frac{E_\mathrm{r}}{E_\mathrm{p}}\left[\frac{t_\mathrm{r}^3}{12} + t_\mathrm{r}\left(\frac{t_\mathrm{p}}{2} + \frac{t_\mathrm{r}}{2} - \bar{z}\right)^2\right] \tag{2}$$

With these two quantities defined, the membrane and bending stress under a remote applied extensional stress, σ^a, are given as follows:

$$\sigma_\mathrm{m}^0 = \sigma^a\left(\frac{1}{1+S} + \frac{t_\mathrm{p}^2\bar{z}^2}{I_t}\right) \tag{3}$$

$$\sigma_\mathrm{b}^0 = \sigma_\mathrm{a}\frac{t_\mathrm{p}^2\bar{z}}{2I_t} \tag{4}$$

For nonlinear bending of a repair of large planar extent with low bending restraint, the neutral axis will move to the load line upon the first instance of loading and the moment carried by the patched structure at the crack plane will vanish. In this case, the stresses on the crack plane simplify to $\sigma_\mathrm{m}^0 = \sigma^a/(1+S)$ and $\sigma_\mathrm{b}^0 = 0$.

2.2. Characterization of crack-bridging springs

To perform the crack-bridging analysis of a repair, it is necessary to model the patch as a set of springs bridging the crack faces. The desired result is a set of spring constants relating the crack-opening stresses to the displacement of the crack face

$$\begin{pmatrix}\sigma_m\\ \sigma_b\end{pmatrix}=\begin{bmatrix}k_{mm} & k_{mb}\\ k_{bm} & k_{bb}\end{bmatrix}\begin{pmatrix}u_m\\ u_b\end{pmatrix} \tag{5}$$

By inversion of Eq. (5), the springs may also be characterized using a compliance matrix, as shown below:

$$\begin{pmatrix}u_m\\ u_b\end{pmatrix}=\begin{bmatrix}c_{mm} & c_{mb}\\ c_{bm} & c_{bb}\end{bmatrix}\begin{pmatrix}\sigma_m\\ \sigma_b\end{pmatrix} \tag{6}$$

The spring compliance coefficients are determined by the analysis of a bonded lap joint that is equivalent in geometry and composition to the cross-section of the repair taken in the region of the crack. The governing equations for a bonded joint under tension and bending are originally from Volkersen (1938), and from Goland and Reissner (1949), and may be expressed in terms of the adhesive stresses as

$$\tau_a'''(x)-\kappa_m^2\tau_a'(x)=0 \tag{7}$$

$$\sigma_a''''(x)+4\kappa_b^4\sigma_a(x)=0 \tag{8}$$

The two characteristic parameters κ_m and κ_b describe the shear and bending response of the joint. By applying the boundary conditions at the crack face, the compliance of the springs bridging the crack faces is derived in Appendix A. The derivation follows the method of Wang and Rose (1997) with the exception of the treatment of the adhesive shear stress boundary condition

$$c_{mm}=\frac{t_p}{\kappa_m}\left(\frac{1}{E_r t_r}+\frac{1}{E_p t_p}+\frac{3(t_r+t_p)}{E_r t_r^2}\right)+\frac{t_p^2}{2\kappa_b D_r}\left(\frac{t_r+t_p}{2}\right) \tag{9}$$

$$c_{mb}=\frac{t_p^2}{\kappa_m}\left(\frac{1}{E_r t_r^2}-\frac{1}{E_p t_p^2}\right)+\frac{t_p^3}{12\kappa_b}\left(\frac{1}{D_r}+\frac{1}{D_p}\right) \tag{10}$$

$$c_{bb}=\frac{t_p^3}{12\kappa_b}\left(\frac{1}{D_r}+\frac{1}{D_p}\right) \tag{11}$$

$$c_{bm}=\frac{t_p^2}{2D_r\kappa_b}\left(\frac{t_r+t_p}{2}\right)\cong 3c_{mb} \tag{12}$$

As found by Wang and Rose, c is asymmetric. This asymmetry is required to satisfy Maxwell's reciprocal theorem, whereby it can be shown that the compliance matrix must obey the relationship $c_{bm}=3c_{mb}$. For a linear system, a set of forces is related to a set of displacements at the points of application of the forces by a symmetric compliance matrix, denoted here as C

$$u=[C]F \tag{13}$$

For a moment acting on a plate, the moment may be equivalently expressed as a pair of forces as shown in Fig. 2.

For the bending and membrane stress distributions shown in Fig. 2, the equivalent forces are given as follows:

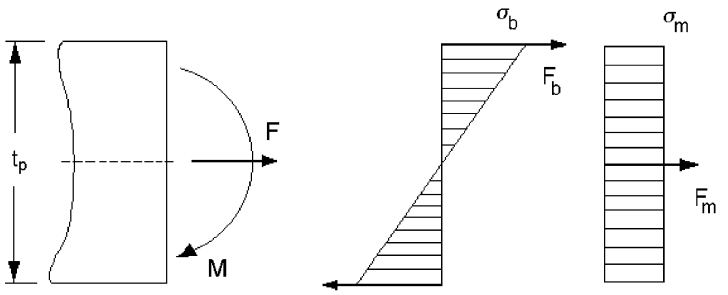

Fig. 2. Equivalency of forces and moments.

$$F_b = \frac{M}{t_p} = \frac{t_p \sigma_b}{6} \tag{14}$$

$$F_m = t_p \sigma_m \tag{15}$$

The compliance matrix may now be expressed in terms of the bending and membrane stresses and displacements

$$\begin{pmatrix} u_m \\ u_b \end{pmatrix} = \begin{bmatrix} C_{mm} & C_{mb} \\ C_{bm} & C_{bb} \end{bmatrix} \begin{pmatrix} F_m \\ 2F_b \end{pmatrix} = t_p \begin{bmatrix} C_{mm} & \frac{C_{mb}}{3} \\ C_{bm} & \frac{C_{bb}}{3} \end{bmatrix} \begin{pmatrix} \sigma_m \\ \sigma_b \end{pmatrix} \tag{16}$$

By Maxwell's reciprocal theorem, $C_{mb} = C_{bm}$. Comparison with Eq. (6) shows that for the spring compliances, $c_{bm} = 3c_{mb}$. Small variations from this relationship will also result from approximations made during the derivation of the bonded joint model. For example, the simple analytical models described by Eqs. (7) and (8) do not include bending moments in the adherends caused by adhesive shear stresses acting at the adherend/adhesive interface. Coupling of extension and bending results only from equilibrium and compatibility requirements employed during the application of the boundary conditions, and small errors will result because the bonded joint model and boundary conditions are inconsistent. Additional minor errors will arise if the adhesive thickness is ignored during derivation of the bonded joint model but included when one determines the boundary conditions.

2.3. Long-crack limit behaviour

Within the crack-bridging analysis, the long-crack limit behaviour of a repair may be determined by energy analysis (Rose, 1982,Wang and Rose, 1997), providing a limiting value for the stress intensity in the plate. To analyze linear coupled bending and extension of a repair, Wang and Rose (1997) have developed an energy method for the separation of the membrane and bending components of the stress intensity in the repaired structure. In this paper, the authors have corrected their method to account for asymmetry of the compliance matrix and the presence of plane strain conditions at the crack tip, as found by Kotousov and Wang (2002) for extension of cracked plates, and by Clark and Romilly (submitted for publication-b) for plate bending. The model is also expressed in terms of the membrane and bending stresses in the plane of the crack to be consistent with the line-spring models developed by Clark and Romilly (submitted for publication-a, submitted for publication-b).

Rose (1981, 1982, 1988) observed that for a very long reinforced crack, the stresses near the crack tip become independent of crack length. The strain energy released with an increment of crack growth may then be found from the difference in stored elastic energy between strips of material far removed from the crack tip. One strip is located over the middle of the long-crack, and its displacement is governed by the stretch of the springs bridging the crack. The other is well away from the crack and is undisturbed by the singular stress field near the crack. The difference in stored energy between the two strips is given by the energy stored in the springs bridging the crack. For a very long reinforced crack, the energy available to drive crack growth will then be equal to the strain energy stored in the springs, and is evaluated as follows (Wang and Rose, 1997):

$$G_\infty = \frac{1}{t_p}\int_{-t_p/2}^{t_p/2} \sigma(z)u(z)\mathrm{d}z = \frac{1}{t_p}\int_{-t_p/2}^{t_p/2} \left(\sigma_m + \sigma_b \tfrac{2z}{t_p}\right)\left(u_m + u_b \tfrac{2z}{t_p}\right)\mathrm{d}z = c_{mm}\sigma_m^2 + 2c_{mb}\sigma_m\sigma_b + \tfrac{1}{3}c_{bb}\sigma_b^2 \tag{17}$$

Based on the results of the generalized plane strain models for extension (Kotousov and Wang, 2002) and bending (Clark and Romilly, submitted for publication-b) of plates, the crack tip must be in a state of plane strain. The strain energy release rate at the outer fibre of the plate will have two components, one for bending and one for extension. Here, K_b and G_b are the stress intensity and strain energy release rate at the outer fibre

$$G_\infty = G_m + \frac{1}{3}G_b = \frac{1-\eta^2}{E_p}\left(K_m^2 + \frac{1}{3}K_b^2\right) \tag{18}$$

The applied stresses are linearly related to the membrane and bending stress intensities

$$\begin{pmatrix} K_{\mathrm{m}}^{\infty} \\ K_{\mathrm{b}}^{\infty} \end{pmatrix} = \begin{bmatrix} d_{\mathrm{mm}} & d_{\mathrm{mb}} \\ d_{\mathrm{bm}} & d_{\mathrm{bb}} \end{bmatrix} \begin{pmatrix} \sigma_{\mathrm{m}} \\ \sigma_{\mathrm{b}} \end{pmatrix} \tag{19}$$

As for the spring compliance matrix, by Maxwell's reciprocal theorem, the authors will demonstrate that $d_{\mathrm{bm}} = 3d_{\mathrm{mb}}$. This is a significant correction to the method of Wang and Rose (1997). Since 1997, it has also been shown by that plane strain conditions will always exist at the crack tip, and the stress intensity at any point along the crack front can be related to the crack face displacement as follows, where r is the distance from the crack tip:

$$K = \lim_{r \to 0} \frac{E_{\mathrm{p}}}{4(1-\eta^2)} \sqrt{\frac{2\pi}{r}} u(r) \tag{20}$$

In the region of the crack tip, Eq. (20) can be rewritten as follows:

$$\lim_{r \to 0} \frac{E_{\mathrm{p}}}{4(1-\eta^2)} \sqrt{\frac{2\pi}{r}} \begin{pmatrix} u_{\mathrm{m}}(r) \\ u_{\mathrm{b}}(r) \end{pmatrix} = \begin{bmatrix} d_{\mathrm{mm}} & d_{\mathrm{mb}} \\ d_{\mathrm{bm}} & d_{\mathrm{bb}} \end{bmatrix} \begin{pmatrix} \sigma_{\mathrm{m}} \\ \sigma_{\mathrm{b}} \end{pmatrix} \tag{21}$$

By the same argument used for the spring compliances (comparison with Eq. (16)) it can be stated that $d_{\mathrm{bm}} = 3d_{\mathrm{mb}}$. Substitution of Eqs. (19) into (18) provides a second expression for G_{∞}, which is a corrected version of that given by Wang and Rose (1997)

$$\frac{E_{\mathrm{p}} G_{\infty}}{1-\eta^2} = \left(d_{\mathrm{mm}}^2 + 3d_{\mathrm{mb}}^2\right)\sigma_{\mathrm{m}}^2 + 2d_{\mathrm{mb}}(d_{\mathrm{mm}} + d_{\mathrm{bb}})\sigma_{\mathrm{m}}\sigma_{\mathrm{b}} + \left(d_{\mathrm{mb}}^2 + d_{\mathrm{bb}}^2/3\right)\sigma_{\mathrm{b}}^2 \tag{22}$$

Repeated differentiation of Eqs. (17) and (22) with respect to the applied stresses will lead to a set of equations solvable for the coefficients of matrix d, as follows:

$$\left(d_{\mathrm{mm}}^2 + 3d_{\mathrm{mb}}^2\right) = c_{\mathrm{mb}} \frac{E_{\mathrm{p}}}{1-\eta^2} \tag{23}$$

$$d_{\mathrm{mb}}(d_{\mathrm{mm}} + d_{\mathrm{bb}}) = c_{\mathrm{mb}} \frac{E_{\mathrm{p}}}{1-\eta^2} \tag{24}$$

$$d_{\mathrm{mb}}^2 + d_{\mathrm{bb}}^2/3 = \frac{1}{3} c_{\mathrm{bb}} \frac{E_{\mathrm{p}}}{1-\eta^2} \tag{25}$$

A unique solution is found by noting that d_{m}, d_{b} must be positive and non-zero, leading to a system of equations solvable for the coefficients of matrix d. It is convenient to define three intermediate variables

$$A = c_{\mathrm{mm}} \frac{E_{\mathrm{p}}}{1-\eta^2}, \quad B = c_{\mathrm{mb}} \frac{E_{\mathrm{p}}}{1-\eta^2}, \quad C = c_{\mathrm{bb}} \frac{E_{\mathrm{p}}}{1-\eta^2} \tag{26}$$

Eqs. (23)–(25) may then be decoupled to form a single equation for d_{mm}

$$\left(d_{\mathrm{mm}} + \sqrt{C - A + d_{\mathrm{mm}}^2}\right)\sqrt{A - d_{\mathrm{mm}}^2} = \sqrt{3}B \tag{27}$$

Eq. (27) has one positive real root, bounded by upper and lower limits given by $\sqrt{A}$ and $\sqrt{A-C}$. The correct value of d_{mm} may be found in this interval using a simple root finding procedure. The remaining coefficients of the d matrix follow:

$$d_{\mathrm{bb}} = \sqrt{C - A + d_{\mathrm{mm}}^2} \tag{28}$$

$$d_{\mathrm{mb}} = \frac{B}{d_{\mathrm{mm}} + d_{\mathrm{bb}}} \tag{29}$$

The resulting long-crack limit membrane and bending stress intensities follow from Eq. (19), and the limit spring displacements are given by Eq. (6). These corrected quantities define the effectiveness of a repair and are essential for the development of an interpolation applicable to repaired cracks of arbitrary length.

2.4. Interpolation for arbitrary crack lengths

This section describes the development of a new engineering model for the stress intensity and crack opening displacement for bridged cracks of arbitrary length. These quantities may be estimated by developing an interpolation between the long-crack limit solutions given by Eqs. (19) and (6), and the nominal solutions for an unreinforced crack. In both cases, the stresses given by Eqs. (3) and (4) are assumed to act to open the crack. The first step is to establish the short-crack limit, or nominal solutions for a through-thickness crack without reinforcing springs. For finite thickness plates, Clark and Romilly (submitted for publication-a, submitted for publication-b) have developed a set of geometry correction factors by using generalized plane strain models for extension and bending of plates. These correction factors account for the through-thickness material properties and the thickness of the plate. For the stress intensity, they take the following form:

$$Y_{\mathrm{k}}^{\mathrm{pres.}}(\alpha) = 1 + \left(\frac{\alpha^{1.5}}{\alpha^{1.5}+1.5}\right)\left(\frac{1}{\sqrt{1-\eta_{\mathrm{p}}^2}} - 1\right) \tag{30}$$

$$Y_{\mathrm{k}}^{\mathrm{shear}}(\alpha) = 1 - \left(\frac{\alpha^{1.2}}{\alpha^{1.2}+3.5}\right)\left(1 - \sqrt{\frac{1+\nu_{\mathrm{p}}}{3+\nu_{\mathrm{p}}}}\right) \tag{31}$$

Using these correction factors, the nominal membrane and bending stress intensity follow:

$$K_{\mathrm{m}}^0 = Y_{\mathrm{k}}^{\mathrm{pres.}}\left(\alpha_{\mathrm{m}}^{\mathrm{pres.}}\right)\sigma_{\mathrm{m}}^0\sqrt{\pi a} = Y_{km}\sigma_{\mathrm{m}}^0\sqrt{\pi a} \tag{32}$$

$$K_{\mathrm{b}}^0 = Y_{\mathrm{k}}^{\mathrm{pres.}}\left(\alpha_{\mathrm{b}}^{\mathrm{pres.}}\right)Y_{\mathrm{k}}^{\mathrm{shear}}\left(\alpha_{\mathrm{b}}^{\mathrm{shear}}\right)\sigma_{\mathrm{b}}^0\sqrt{\pi a} = Y_{\mathrm{kb}}\sigma_{\mathrm{b}}^0\sqrt{\pi a} \tag{33}$$

Eqs. (34) and (35) provide the necessary geometry correction factors for the maximum displacement of the crack faces, which occurs at the centre of the crack.

$$Y_{\mathrm{d}}^{\mathrm{pres.}}(\alpha) = 1 + \left(\frac{\alpha^{1.5}}{\alpha^{1.5}+2.5}\right)\left(\frac{1}{1-\eta_{\mathrm{p}}^2} - 1\right) \tag{34}$$

$$Y_{\mathrm{d}}^{\mathrm{shear}}(a) = 1 - \left(\frac{\alpha^{1.3}}{\alpha^{1.3}+5}\right)\left(1 - \frac{1+\nu_{\mathrm{p}}}{3+\nu_{\mathrm{p}}}\right) \tag{35}$$

Without any crack-bridging springs, the extensional and bending displacements of the crack faces under the action of the crack-opening stresses, σ_{m}^0 and σ_{b}^0, will then be

$$u_{\mathrm{m}}^0 = 2Y_{\mathrm{d}}^{\mathrm{pres.}}\left(a_{\mathrm{m}}^{\mathrm{pres.}}\right)\frac{\sigma_{\mathrm{m}}^0(1-\eta_{\mathrm{p}}^2)}{E_{\mathrm{p}}}a = 2Y_{\mathrm{dm}}\frac{\sigma_{\mathrm{m}}^0(1-\eta_{\mathrm{p}}^2)}{E_{\mathrm{p}}}a \tag{36}$$

$$u_{\mathrm{b}}^0 = 2Y_{\mathrm{d}}^{\mathrm{pres.}}\left(\alpha_{\mathrm{b}}^{\mathrm{pres.}}\right)Y_{\mathrm{d}}^{\mathrm{shear}}\left(\alpha_{\mathrm{b}}^{\mathrm{shear}}\right)\frac{\sigma_{\mathrm{m}}^0(1-\eta_{\mathrm{p}}^2)}{E_{\mathrm{p}}}a = 2Y_{\mathrm{db}}\frac{\sigma_{\mathrm{m}}^0(1-\eta_{\mathrm{p}}^2)}{E_{\mathrm{p}}}a \tag{37}$$

Each of the correction factors is a function of α, a normalized crack length that accounts for the effects of the transverse properties and thickness of the plate. The three normalized crack lengths characterize the effects of transverse normal stresses in extension, transverse normal stresses in bending, and transverse shear in bending, respectively,

$$\alpha_{\mathrm{m}}^{\mathrm{pres.}} = \frac{2a}{t_{\mathrm{p}}}\sqrt{3\left(1+\nu_{\mathrm{p}}^{\mathrm{z}}\right)} \tag{38}$$

$$\alpha_{\mathrm{b}}^{\mathrm{pres.}} = \frac{2a}{t_{\mathrm{p}}}\frac{\nu_{\mathrm{p}}^{\mathrm{z}}}{\eta}\sqrt{\frac{15E_{\mathrm{p}}}{G_{\mathrm{p}}^{\mathrm{z}}}} \tag{39}$$

$$\alpha_{\mathrm{b}}^{\mathrm{shear}} = \frac{2a}{t_{\mathrm{p}}}\sqrt{\frac{6G_{\mathrm{p}}^{\mathrm{z}}(3+\nu_{\mathrm{p}})}{E_{\mathrm{p}}}} \tag{40}$$

These nominal solutions for the stress intensities and displacements provide the short-crack limit solution. The long-crack limit stress intensities may be calculated using Eq. (19), and the corresponding long-crack limit displacements are given by Eq. (6). At this point the authors propose a new method of interpolation between these limits to establish the state of a reinforced crack of arbitrary length. For the case of coupled extension and bending, a very effective interpolation may be achieved by considering the stiffness of both the cracked plate and the crack-bridging springs. Eqs. (36) and (37) may be inverted to develop expressions for the stiffness of the cracked plate

$$k_{\mathrm{m}}^{\mathrm{p}} = \frac{\sigma_{\mathrm{m}}^{0}}{u_{\mathrm{m}}^{0}} = \left(\frac{E_{\mathrm{p}}}{1-\eta_{\mathrm{p}}^{2}}\right)\frac{1}{2Y_{\mathrm{dm}}a} \tag{41}$$

$$k_{\mathrm{b}}^{\mathrm{p}} = \frac{\sigma_{\mathrm{m}}^{0}}{u_{\mathrm{b}}^{0}} = \left(\frac{E_{\mathrm{p}}}{1-\eta_{\mathrm{p}}^{2}}\right)\frac{1}{2Y_{\mathrm{db}}a} \tag{42}$$

A stiffness matrix for the as-reinforced crack may now be developed by considering the crack and the patch as a set of springs acting in parallel. The result is an as-reinforced stiffness matrix applicable to repaired cracks of arbitrary length

$$\begin{pmatrix} \sigma_{\mathrm{m}}^{0} \\ \sigma_{\mathrm{b}}^{0} \end{pmatrix} = \begin{bmatrix} k_{\mathrm{mm}} + k_{\mathrm{m}}^{\mathrm{p}} & k_{\mathrm{mb}} \\ k_{\mathrm{bm}} & k_{\mathrm{bb}} + k_{\mathrm{b}}^{\mathrm{p}} \end{bmatrix} \begin{pmatrix} u_{\mathrm{m}}^{\mathrm{r}} \\ u_{\mathrm{b}}^{\mathrm{r}} \end{pmatrix} \tag{43}$$

By inverting the combined stiffness matrix of Eq. (43), a new compliance matrix may be generated for any particular crack length that accounts for the stiffness of the cracked plate

$$\begin{pmatrix} u_{\mathrm{m}}^{\mathrm{r}} \\ u_{\mathrm{b}}^{\mathrm{r}} \end{pmatrix} = \begin{bmatrix} c_{\mathrm{mm}}^{\mathrm{r}} & c_{\mathrm{mb}}^{\mathrm{r}} \\ c_{\mathrm{bm}}^{\mathrm{r}} & c_{\mathrm{bb}}^{\mathrm{r}} \end{bmatrix} \begin{pmatrix} \sigma_{\mathrm{m}}^{0} \\ \sigma_{\mathrm{b}}^{0} \end{pmatrix} \tag{44}$$

The as-reinforced crack face displacements can now be calculated directly, and the as-reinforced membrane and bending stress intensity may be calculated by applying the new compliance matrix to the energy method described in Section 2.3. This is a new application of the energy method, which has in the past only been used to calculate long-crack limit solutions. This method of interpolation does not require any assumptions regarding the ratio of the membrane and bending components, overcoming a significant problem with the method of Wang et al., 1998.

This new approach to the interpolation allows for the simplified analysis of linear coupled bending and extension of a repair and includes the effects of transverse normal and shear stresses and accompanying shear deflections. It is a valuable tool for patch design and damage tolerance. In subsequent sections, this new interpolation model will be validated against a numerical line-spring model for generalized plane strain plates and against a three-dimensional finite element model of a bonded composite repair.

3. A line-spring model for crack-bridging

In this section we combine the generalized plane strain crack-bridging models for extension and bending (Clark and Romilly, submitted for publication-a, submitted for publication-b) to address the problem of a crack bridged by coupled springs. The results will be used to validate the closed-form equations developed in Section 2 above. The springs bridging the crack are characterized by Eq. (5), i.e. the stiffness matrix relating the membrane and bending stresses to the crack face displacements. Using an approach similar to that of Wang and Rose (1999), the line-spring models for extension and bending may be combined to include the effect of the coupling springs. The significant differences in the current approach are the use of the generalized plane strain plate models and the choice to express the bending moment and displacement in terms of the crack face displacement and the bending stress in the outer fibre of the plate. The generalized plane strain plate models lead to additional terms that account for pressurization and transverse shear about the crack tip. This leads to the following set of coupled Fredholm integral equations with hyper-singular integrands that are solv-

able for the crack face displacements. The left side of the equation is the net crack opening stress along the crack face, and the right side describes the reaction of the plate

$$\sigma_{\mathrm{m}}^{0}(y)-k_{\mathrm{mm}}u_{\mathrm{m}}(y)-k_{\mathrm{mb}}u_{\mathrm{b}}(y)=\frac{-1}{2\pi}\int_{-a}^{a}\frac{E_{\mathrm{p}}u_{\mathrm{m}}(t)}{1-\eta^{2}}\left(\frac{1}{(t-y)^{2}}+\eta^{2}\left(\kappa_{\mathrm{m}}^{\mathrm{pres.}}\right)^{2}L^{\mathrm{pres.}}\left(\kappa_{\mathrm{m}}^{\mathrm{pres.}}|t-y|\right)\right)\mathrm{d}t \tag{45}$$

$$\sigma_{\mathrm{b}}^{0}(y)-k_{\mathrm{bb}}u_{\mathrm{b}}(y)-k_{\mathrm{bm}}u_{\mathrm{m}}(y)=\frac{-1}{2\pi}\int_{-a}^{a}\frac{E_{\mathrm{p}}u_{\mathrm{b}}(t)}{1-\eta^{2}}\times\left(\frac{1}{(t-y)^{2}}+\frac{\left(\kappa_{\mathrm{b}}^{\mathrm{shear}}\right)^{2}}{2}\frac{1-\eta^{2}}{1+v}L^{\mathrm{shear}}\left(\kappa_{\mathrm{b}}^{\mathrm{shear}}|t-y|\right)+\left(\kappa_{\mathrm{b}}^{\mathrm{pres.}}\right)^{2}\eta^{2}L^{\mathrm{pres.}}\left(\kappa_{\mathrm{b}}^{\mathrm{pres.}}|t-y|\right)\right)\mathrm{d}t \tag{46}$$

In Eqs. (45) and (46), the following parameters characterize the through-thickness properties of the plate:

$$\kappa_{\mathrm{m}}^{\mathrm{pres.}}=\frac{2}{t_{\mathrm{p}}}\sqrt{\frac{3E_{z}}{G_{z}(1-\eta_{\mathrm{p}}^{2})}} \tag{47}$$

$$\kappa_{\mathrm{b}}^{\mathrm{pres.}}=\frac{2\nu_{\mathrm{p}}^{z}}{t_{\mathrm{p}}\eta_{\mathrm{p}}}\sqrt{\frac{15E}{G_{z}(1-\eta_{\mathrm{p}}^{2})}} \tag{48}$$

$$\kappa_{\mathrm{b}}^{\mathrm{shear}}=\frac{2}{t_{\mathrm{p}}}\sqrt{\frac{3G_{z}}{G}} \tag{49}$$

The functions $L^{\mathrm{pres.}}(z)$ and $L^{\mathrm{shear}}(z)$ describe the effects of pressurization and transverse shear stresses acting near the crack tip. If the $L^{\mathrm{pres.}}(z)$ functions are neglected, the line-spring model will take the form for classical plane strain extension and the form for plane strain plate bending with shear deflections (i.e. plate bending according to the Mindlin formulation). If the term $L^{\mathrm{shear}}(z)$ is also removed, then the effects of transverse shear stresses and the accompanying shear deflections will be removed. The formulation of Wang and Rose (1999) can be recovered by neglecting the pressurization terms, removing the plane-strain modification of the Young's modulus, and using isotropic rather than transversely isotropic material properties. The functions $L^{\mathrm{pres.}}(z)$ and $L^{\mathrm{shear}}(z)$ have the following form, where K_{n} are various orders of modified Bessel functions of the second kind

$$L^{\mathrm{pres.}}(z)=2\left[1+\frac{3}{z^{2}}\right]K_{2}(z)-\frac{12}{z^{4}}-\frac{1}{z^{2}} \tag{50}$$

$$L^{\mathrm{shear}}(z)=-\frac{48}{z^{4}}+\frac{4}{z^{2}}+4(K_{2}(z)-K_{0}(z))+\frac{24}{z^{2}}K_{2}(z) \tag{51}$$

The domain of the integration in Eqs. (58) and (59) may be normalized with respect to the half-crack length, a, and the displacements expanded using Chebyshev polynomials of the second kind

$$U_{i}(r)=\sin((i+1)\cos^{-1}(r))/\sqrt{1-r^{2}} \tag{52}$$

For this set of orthogonal polynomials, the weight function is given by

$$W(r)=\sqrt{1-r^{2}} \tag{53}$$

Given this expansion, the crack face displacements may now be decomposed as follows:

$$u_{\mathrm{m}}(r)=\sum_{i}W(r)U_{i}(r)f_{i} \tag{54}$$

$$u_{\mathrm{b}}(r)=\sum_{i}W(r)U_{i}(r)g_{i} \tag{55}$$

Choosing a set of collocation points, a coupled linear system may now be defined from Eqs. (45) and (46), which may be solved for the expansion coefficients

$$\begin{Bmatrix} \overline{\sigma_m} \\ \overline{\sigma_b} \end{Bmatrix} = \begin{bmatrix} A & B \\ C & D \end{bmatrix} \begin{Bmatrix} f \\ g \end{Bmatrix} \tag{56}$$

In this system, the matrix coefficients have the following definitions:

$$A_{i,j} = \frac{E_p}{1-\eta^2}\left(\frac{i+1}{2}U_j(r_i) - \frac{\eta^2\left(a\kappa_m^{\text{pres.}}\right)^2}{2\pi}L_{i,j}^{\text{pres.}}\right) + ak_{mm}W(r_i)U_j(r_i) \tag{57}$$

$$B_{i,j} = ak_{mb}W(r_i)U_j(r_i) \tag{58}$$

$$C_{i,j} = \frac{E_p}{1-\eta^2}\left(\frac{i+1}{2}U_j(s_i) - \frac{\left(a\kappa_b^{\text{shear}}\right)^2}{4\pi}\left(\frac{1-\eta^2}{1+\nu}\right)L_{i,j}^{\text{shear}} - \frac{\left(a\kappa_b^{\text{pres.}}\right)^2\eta^2}{2\pi}L_{i,j}^{\text{pres.}}\right) + ak_{bb}W(s_i)U_j(s_i) \tag{59}$$

$$D_{i,j} = ak_{bm}W(r_i)U_j(r_i) \tag{60}$$

Analytical solutions exist for the logarithmic parts of $L^{\text{shear}}(z)$ and $L^{\text{pres.}}(z)$, but the regular parts require numerical integration. The term $V_{i,j}$ arises from the logarithmic singularity, and may be solved analytically, as demonstrated by Joseph and Erdogan (1987, 1989) and by Wang and Rose (1999). To evaluate the regular part, the authors used Gauss–Chebyshev quadrature, as suggested.

$$L_{i,j}^{\text{shear}} = \int_{-1}^{1}\left[L^{\text{shear}}(a\kappa^{\text{shear}}|r_i - s|) - \ln(|r_i - s|)\right]W(s)U_j(s)\mathrm{d}s + V_{i,j} \tag{61}$$

$$L_{i,j}^{\text{pres.}} = \int_{-1}^{1}\left[L^{\text{pres.}}(a\kappa^{\text{pres.}}|r_i - s|) + \frac{3}{4}\ln(|r_i - s|)\right]W(s)U_j(s)\mathrm{d}s - \frac{3}{4}V_{i,j} \tag{62}$$

$$V_{i,j} = \int_{-1}^{1}\ln|r_i - s|W(s)U_j(s)\mathrm{d}s = \begin{cases} -\frac{\pi}{2}\left[-r_i^2 + \frac{1}{2} + \ln 2\right] & j = 0 \\ -\frac{\pi}{2}\left[\frac{T_j(r_i)}{j} - \frac{T_{j+2}(r_i)}{j+2}\right] & j > 0 \end{cases} \tag{63}$$

For the generalized plane strain plate models, the stress intensities in extension and bending may be found from the expansion coefficients in the following manner:

$$K_m^n = \frac{E\sqrt{\pi a}}{2(1-\eta^2)}\sum_{i=0}^{N}(i+1)f_i \tag{64}$$

$$K_b^n = \frac{E\sqrt{\pi a}}{2(1-\eta^2)}\sum_{i=0}^{N}(i+1)g_i \tag{65}$$

These stress intensity results will be compared to the interpolation model results and finite element results in Section 4.1.

The displacement of the crack faces may be related to the line-forces carried by the springs via Eq. (5). Expressing the membrane and bending stresses as their line-force equivalents:

$$N_x(y) = 2h(k_{mm}u_m(y) + k_{mb}u_b(y)) \tag{66}$$

$$M_x(y) = \frac{2}{3}h^3(k_{bm}u_m(y) + k_{bb}u_b(y)) \tag{67}$$

Given the crack face displacements, these expressions for loading may be used to predict fatigue cracking and/or rupture of the springs (i.e. the patch materials) bridging the crack faces as required for patch design and/or damage tolerance assessment.

4. Comparison to finite element models

In this section, finite element models are used to determine the effectiveness of the closed-form equations. The stress intensities and crack face displacements calculated using the closed-form equations and the line-spring model are compared to a fully three-dimensional model of a bonded composite repair, the nominal stresses under the repair and the compliance of the repair as it bridges the crack are investigated by the use

of two-dimensional bonded joint finite element models, and the three-dimensional finite element model is used to examine the nonlinear response of the structure.

4.1. Stress intensity and crack face displacements

The authors have developed three-dimensional solid finite element models representing the AMRL (Australian Maritime Research Laboratory) specimen, a specimen type that has been widely adopted for the investigation of the mechanics of bonded repairs (e.g. Baker 1993). The models have been validated against mechanical testing of an instrumented specimen, during which strains were measured at nearly 100 positions on the patch and repaired plate, including 40 strain gauges applied to the face of the composite repair as it bridged the crack (Clark and Romilly, 2002). Fig. 3(a) shows the model in a large-plate configuration for a crack length of 160 mm. Note that due to symmetry only one-quarter of the plate is modelled with the appropriate symmetry boundary conditions applied. This model geometry is designed to test the closed-form equations and line-spring model for the idealized case from which they where derived. Fig. 3(b) shows a close-up of the elements near the crack tip, with some elements removed to show the repair patch, epoxy, and plate layers. The crack face is identified by the cross-hatched region in Fig. 3.

The finite element models were developed using the ANSYS finite element software, utilizing three-dimensional 20-node brick elements and 15-node wedges. The wedge elements employ quarter-point mid-side nodes to model the singularity at the crack tip, from which the stress intensity was calculated using the stresses at three integration points in the wedges ahead of the crack tip. This stress-based approach allowed for accurate evaluation the stress intensity as it varied through the thickness of the plate. Validation models demonstrated stress intensities accurate to within 2% compared to theoretical models corrected for through-thickness effects. The material properties and dimensions applied in the finite element models are given in Table 1. Note that for

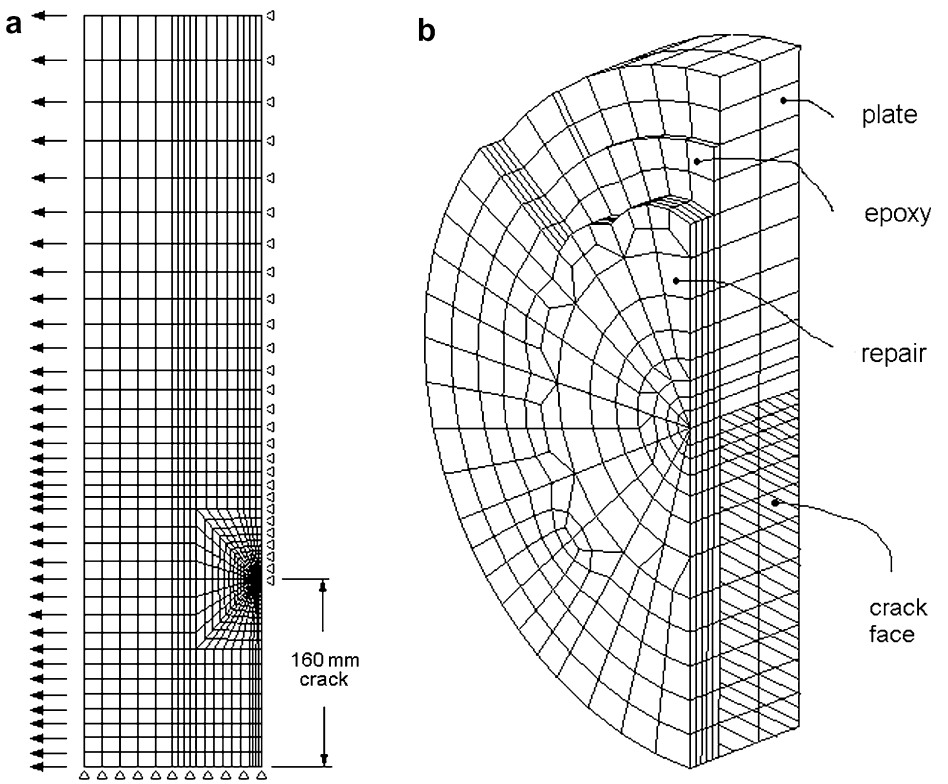

Fig. 3. Three-dimensional finite element model of a repair.

Table 1
Material properties and dimensions

Property	Boron/epoxy patch	FM-73M adhesive	2024-T3 aluminum plate
Elastic modulus, E	210 GPa	2.14 GPa	72.4 GPa
Shear modulus, G	7.24 GPa	0.805 GPa	27.2 GPa
Poisson's ratio, υ	0.21	0.33	0.33
Thermal expansion, α	4.61 με/°C	50.0 με/°C	23.45 με/°C
Thickness, t	0.924 mm	0.25 mm	3.125 mm

the purposes of this paper, the patch was modelled as an isotropic solid to remove the complicating effects of transverse shear and peel deformations as would otherwise exist in an orthotropic composite.

The membrane and bending stress intensities are the average stress intensity and the stress intensity at the outer fibre of the plate, respectively, as found from the average and the first moment of the stress intensity taken through the thickness of the plate. These quantities were calculated using a linear least-squares fit to the stress intensities found at the integration points through the thickness of the plate. To determine the actual transverse variation of the stress intensity through the thickness of the plate would require the use of many elements, as a thin boundary layer exists at the top and bottom surfaces. However, convergence studies have shown that few elements are required to obtain accurate values for the plate-averaged quantities, k_m and k_b. The three-dimensional finite element models employ two elements through the thickness of the plate, enough to ensure that errors due to through-thickness mesh refinement are much smaller than the 2% error resulting from stress intensity determination.

Figs. 4 and 5 show the membrane and bending stress intensities predicted by the interpolation model and by the line-spring model when compared to the large plate finite element model, under a remote applied stress of 1 MPa. The nominal results are the membrane and bending stress intensities that would arise if the patch only acted to reduce the stresses in the underlying plate but did not act to restrict the opening of the crack. For both the interpolation model and the line-spring model, the nominal stresses were calculated using plane strain results from a two-dimensional finite element model, as described in Section 4.2, and the spring stiffnesses were calculated using the plane strain analytical results from Section 2.2.

The interpolation and line-spring models provide very similar results for short cracks but diverge when the crack length becomes large. For long-cracks, the line-spring model develops errors due to the increasing importance of the higher order Chebychev polynomials and the errors arising from numerical integration of the regular parts of the hyper-singular integrals. For relatively short cracks with $a < 50$ mm, the interpolation model membrane stress intensity is lower by less than 2% and the interpolation model bending stress intensity is higher by as much as 10% when compared to the FEM results. This 10% error can be attributed in roughly equal parts to three sources. First, Eq. (31) slightly over-predicts the nominal stress intensity for

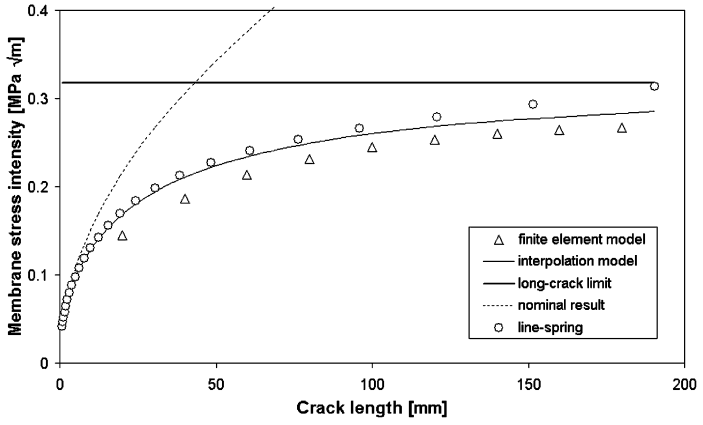

Fig. 4. Membrane stress intensity.

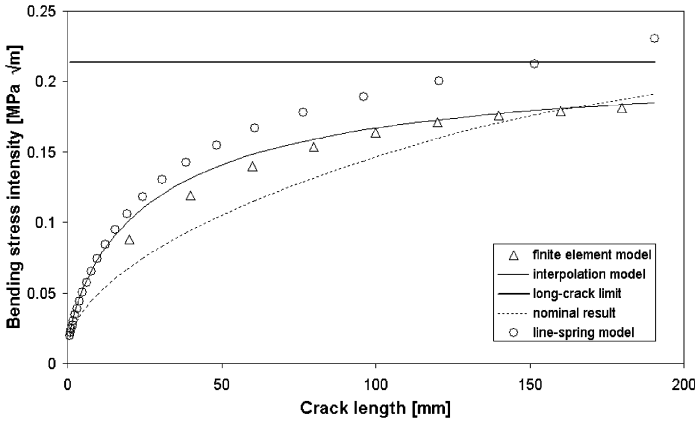

Fig. 5. Bending stress intensity.

this plate, next, very small variations from Maxwell's reciprocal theorem that arise due to simplifications made during the development of the spring compliance matrix lead to disproportionately large errors for this crack length and last, the interpolation method is approximate and errors of up to 5% should be expected. The finite element results are generally lower than those calculated using either analytical model, a difference that could arise from a number of sources. Using the limited academic version of ANSYS, it is difficult to include enough elements in the adhesive layer near the crack, and at the same time model a repaired plate of large planar extent. An insufficiently dense mesh would cause the repair to appear to be overly stiff and artificially reduce the stress intensity and crack face displacement.

Figs. 6 and 7 compare the membrane and bending crack face displacements calculated using the interpolation model and the line-spring model to the results of the large-plate finite element model.

The crack displacement results follow a similar trend to that observed for the stress intensities. For short cracks with $a < 50$ mm, both the interpolation model membrane and bending displacements are lower by less than 4% when compared to the FEM results. For long-cracks the interpolation and line-spring model results diverge for the same reasons as stated above. In both cases, interpolation provides reasonable results, and the long-crack limits established by the energy analysis are obeyed. This contradicts the findings of Wang and Rose (1997), who, by comparison to a three-dimensional finite element model, observed that the energy method significantly over-predicts the bending stress intensity and is not a useful approach. This supports the validity of the modifications described in Section 2, i.e. that the crack tip must be considered to be in a state of plane strain and that Maxwell's reciprocal theorem must be satisfied in the manner shown. In the next

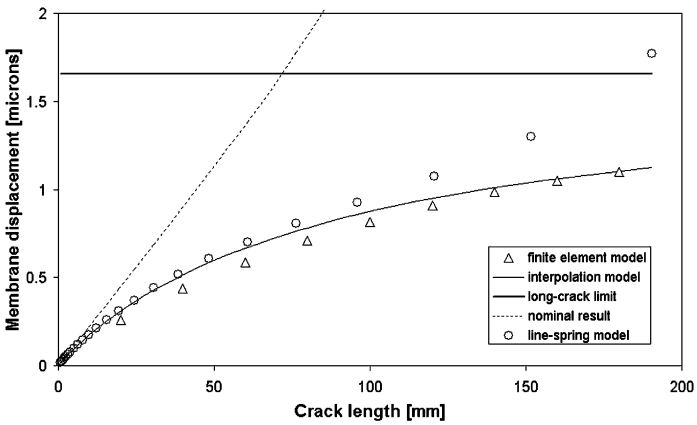

Fig. 6. Membrane crack face displacement.

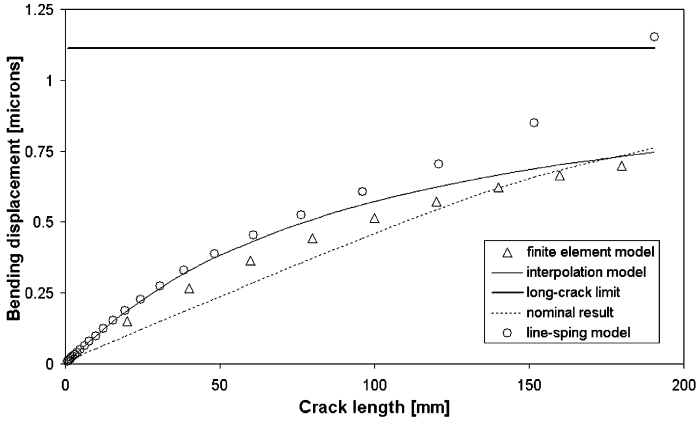

Fig. 7. Bending crack face displacement.

section, a two-dimensional finite element model will be used to examine the effectiveness of the means used to calculate the crack opening pressures and the definition of the spring constants.

4.2. Spring stiffness and nominal stress determination

The composite beam model used to calculate the nominal stresses under a repair is, strictly speaking, only applicable to a very large patch without boundary conditions that lead to restraint against bending. The effect of a finite patch applied to a plate with rotational constraints at the grips can be estimated using finite element analysis. Using the same materials and geometry as were used for the large plate finite element model, a two-dimensional finite element model has been developed for this purpose and to calculate the compliance of the repair as it bridges the crack. This model has been validated against load-deflection curves, strain gauge data, and lateral deflections from experiments (Clark and Romilly, 2003). Fig. 8 shows the finite element mesh and boundary conditions for two configurations of the model, one with a crack under the patch (top), and an uncracked version used to calculate the nominal stresses under the repair (bottom).

In this particular analysis, the bonded repair is assumed to be isotropic to eliminate composite deformations that cannot be predicted using the bonded joint equations presented in this paper. Fig. 9 shows the nominal stresses predicted by the closed-form equations for a remote applied stress of 1 MPa. Both the finite element and closed-form equation results are shown for two cases: plane stress and plane strain. It is likely that the correct case is the intermediate one of generalized plane strain, where the structure is allowed to deform uniformly in the transverse direction. For the AMRL geometry, it is seen that the closed-form equations provide reasonable results, but that there are sufficient differences to account for the errors observed in the comparison of the line-spring and interpolation model results to the three-dimensional finite element

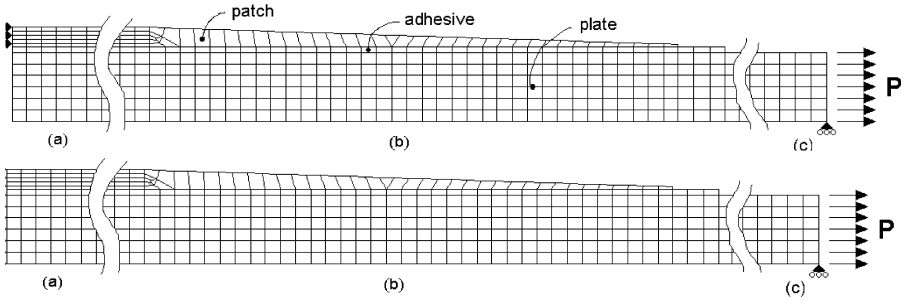

Fig. 8. FE mesh showing the (a) cracked, (b) tapered, and (c) grip regions.

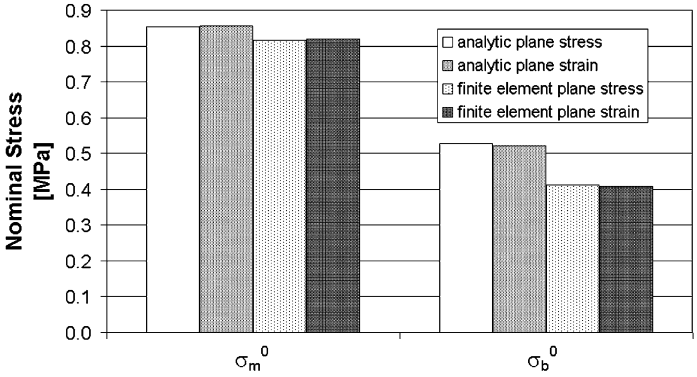

Fig. 9. Nominal stresses.

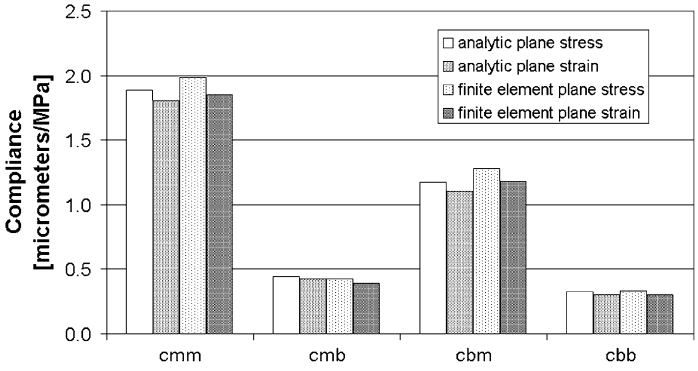

Fig. 10. Spring compliances.

results. The closed-form equations are seen to generally over-predict the nominal stresses, which would lead to an over-estimate of the stress intensities and crack face displacements.

The other factor that would affect the interpolation results is the calculation of the spring compliances. Fig. 10 shows a comparison of the spring compliances predicted by the closed-form equations and the finite element model. These displacements were derived by separately applying a uniform membrane stress and a linearly varying bending stress to the face of the crack in the two-dimensional finite element model shown above. Again, the results are shown for two cases, plane stress and plane strain.

The closed-form equations are shown to provide very reasonable results, generally slightly under-estimating the stiffness of the patch when compared to finite elements. In the generation of Figs. 4, 6 and 7, the plane stress closed-form equations were used, which when compared to the plane strain results, may demonstrate a slight over-estimate of the compliance of the repair. As in the determination of the nominal stresses, the actual state of the repair in the idealized large plate case is likely to be one of generalized plane strain, and intermediate to the plane stress and plane strain results. Accordingly, it is difficult to precisely determine what role the spring stiffness equations might contribute to the differences observed between the three-dimensional finite element models and the interpolation and line-spring models.

4.3. Geometrically nonlinear bending and extension

Wang and Rose (1997) have suggested that nonlinear bending of repairs can be analyzed by calculating the nominal stresses under the repair considering the effects of stress-stiffening, and then applying these stresses as crack-opening stresses in a crack-bridging analysis similar to the one provided above. The assumption is that the additional displacements caused by the presence of the crack are small and localized and will not greatly

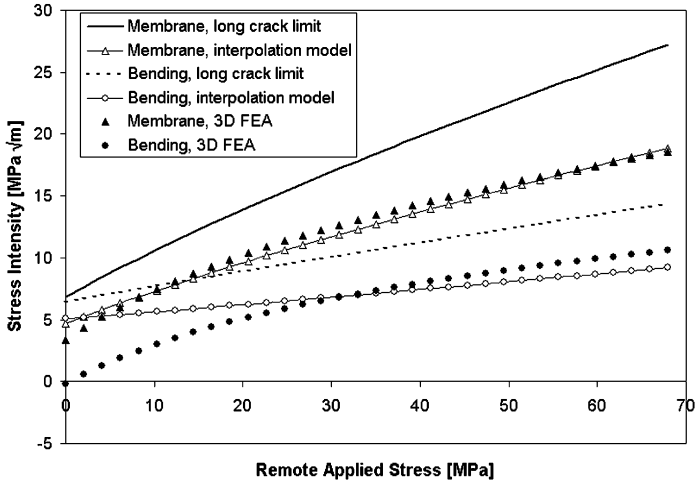

Fig. 11. Nonlinear variation of the membrane stress intensity.

affect the results. To test this approach, the authors have compared the results of a geometrically nonlinear solution of the large-plate three-dimensional solid finite element model to those predicted by the interpolation model. Here, the nominal stresses were determined from a nonlinear solution of the two-dimensional bonded joint model described in the previous section. In this case, the authors have also included the effects of thermal residual strains arising during the curing process, and have used a crack length of 40 mm (see Fig. 11).

It is apparent that this approach leads to reasonable results for large loads, when the repair has largely moved toward the load line and lateral deflections become less of a factor, but leads to poor results under small loads, where nonlinear behaviour dominates. This effect is not predicted using the method presented by Wang and Rose. It should be noted that the AMRL specimen was not designed to test unbalanced repairs. It employs a very thick plate and uses a patch of relatively small planar area relative to what would be used for most aircraft structures, and hence is a very extreme test of the technology. It is possible that the approach might work for a large and thin patch applied to a much thinner plate, where the effects of induced bending will be smaller. Accordingly, such a technique needs to be applied with caution (i.e. validated on a case-by-case basis) or not at all. It assumes that the linear concept of superposition can be applied to a nonlinear problem.

5. Results and discussion

Through comparison with three-dimensional finite element results, it has been shown that the line-spring and new interpolation models capture the crack-bridging behaviour of a repair. Also through comparison with finite element analysis, it has been shown that the composite beam model may lead to some inaccuracies in the determination of the nominal stresses acting under the repair. Factors affecting its applicability include the length of the repair, the support conditions, and the planar stress state assumed to exist in the repair (i.e. plane stress or plane strain conditions). Some additional complicating effects that have not been investigated for the case of linear coupled bending and extension are the shape of the patch (whereby patches of finite planar geometry are known to generally increase the stresses in the region of the repair) and the effects of a highly anisotropic composite patch. Another pressing issue is that, while the common bonded joint model presented in this paper proved adequate in the case of an isotropic repair, the composite nature of a real repair is a complicating factor in the determination of the compliance of the repair as it bridges the crack. The modelling of such a hybrid bonded joint is complicated by many secondary effects such as shear and peel (transverse normal) deformations that act to increase the compliance of the repair, pressurization of the adhesive due to peel stresses, the plane state of the adherends and the adhesive, and the complementary shear deformations resulting from the rapidly changing bending stresses in the patch and plate. These effects can be particularly impor-

tant in the prediction of failure of the repair by disbonding, where the peel and shear stresses in the adhesive must be known. The alternative to accurately determining the adhesive stresses is to calculate the strain energy release rate of the bonded joint system, which may be safely compared to experimental results for a similar specimen under similar loading conditions to predict fracture and fatigue, but is not directly comparable to any adhesive material property. This would necessitate a significant amount of testing for each new combination of materials or for new loading combinations, which is currently the norm in the development of composite airframe structures.

An additional issue that has not been addressed is the crack closure phenomenon that occurs on the compressive side of the bending plate when the applied tensile loads are not sufficient to prevent closure. This has been identified by Duong and Wang (2004) as one of the principal impediments to the prediction of the rate of failure of a cracked plate under tensile and bending loads. They have proposed an effective or modified stress intensity to account for combined bending and tensile loads, but admit that their technique requires further work before it can be used generally. The authors hope that the development of the generalized plane strain plate line-spring models will prove useful in the analysis of this phenomenon. Crack closure would pose a nonlinear contact problem, which could be examined by using a one-dimensional finite element mesh along the crack face instead of using Chebychev polynomials to obtain a numerical solution. Without a method to address this issue, experimental verification or very conservative means should be employed in the prediction of failure, such as simply adding the membrane and bending stress intensities and comparing them to the critical stress intensity for the material or by using them together in the Paris equation. This approach should prove to be conservative, as it will effectively over-predict the energy available for fracture.

The final issue addressed within this paper was the analysis of nonlinear deformations of the repair under extensional loads. It was demonstrated that a linear crack-bridging analysis employing stresses found by a geometrically nonlinear bending analysis of the uncracked structure is generally not adequate for the prediction of the stress intensity of the repaired crack. Alternative means are required, whereby nonlinear analysis must be used to establish the long-crack limit stress intensity factors and crack opening displacements.

6. Concluding remarks

In this paper, the authors have, based on a corrected form of the energy method of Wang and Rose, developed a new interpolation model applicable to the analysis of bridged cracks under combined tension and bending. The interpolation model has been tested against a line-spring model of for a generalized plane strain cracked plate and a full three-dimensional analysis of a repaired plate, and proven to be very accurate for the AMRL specimen geometry. Some deficiencies have been noted in the methods used to determine the nominal stresses acting in the regions of the repair and in the extension of linear crack-bridging models to the analysis of unbalanced repairs experiencing stress stiffening, and accordingly the authors urge bonded repair designers to verify their results against finite element models or experiments when thick plates or repairs of limited planar dimensions are analysed. It has also been noted that for an anisotropic composite repair, standard bonded joint models may not be adequate for the determination of the spring compliances or the prediction of disbonding and fracture. Prediction of the rate of failure or ultimate load of the structure is also complicated by the lack of an adequate and widely accepted means of translating the stress intensities or adhesive stresses into crack or disbond fracture or growth rates, which will continue to require the structural testing of repairs (and composite structures in general) to determine their suitability for service.

Appendix A. Calculation of spring compliances

The characteristic parameters governing the response of the bonded joint are given as follows:

$$\kappa_{\mathrm{m}}^2 = \frac{4G_{\mathrm{a}}}{t_{\mathrm{a}}}\left(\frac{1}{E_{\mathrm{p}}t_{\mathrm{p}}} + \frac{1}{E_{\mathrm{r}}t_{\mathrm{r}}}\right) \tag{A.1}$$

$$\kappa_{\mathrm{b}}^4 = \frac{E_{\mathrm{a}}}{t_{\mathrm{a}}}\left(\frac{1}{D_{\mathrm{p}}} + \frac{1}{D_{\mathrm{r}}}\right) \tag{A.2}$$

The general solutions to Eqs. (7) and (8), considering only those parts that vanish as $x \to \infty$, are given by

$$\tau_a(x) = Ae^{-\kappa_m x} \tag{A.3}$$

$$\sigma_a(x) = [B\cos(\kappa_b x) + C\sin(\kappa_b x)]e^{-\kappa_b x} \tag{A.4}$$

The integration constants are determined by the boundary conditions of the joint. Of interest are the displacements under the action of an applied force and moment acting on the plate

$$N_p(0) = -\sigma_m^0 t_p \tag{A.5}$$

$$M_p(0) = -\sigma_b^0 t_p^2/6 \tag{A.6}$$

The force and moment acting on the reinforcement are determined considering equilibrium

$$N_r(0) = \sigma_m^0 t_p \tag{A.7}$$

$$M_r(0) = \sigma_b^0 t_p^2/6 + \sigma_m^0 t_p(t_p + t_r)/2 \tag{A.8}$$

The final condition is symmetry, which requires the transverse shear forces to vanish

$$V_p(0) = V_r(0) = 0 \tag{A.9}$$

The stresses may be expressed in terms of the boundary conditions using the adhesive constitutive equations. The process is identical to that of Wang and Rose (1999), with the exception that here the shear forces are made to vanish according to (A9). Wang and Rose included an extra term to balance the shear stress at the edge of the adhesive layer, $\tau_a(0)$, which is of minor consequence and will vanish in a real joint. Eq. (A9) requires $C = -B$, and the remaining constants are found to be

$$A\frac{\kappa_m t_a}{G_a} = \left[\frac{1}{E_r t_r} + \frac{1}{E_p t_p} + \frac{3(t_r + t_p)}{E_r t_r^2}\right]\sigma_m^o t_p + \left[\frac{1}{E_r t_r^2} - \frac{1}{E_p t_p^2}\right]\sigma_b^0 t_p^2 \tag{A.10}$$

$$B\frac{\kappa_b^2 D_r t_a}{E_a} = \left(\frac{t_r + t_p}{2}\right)\sigma_m^0 t_p + \frac{1}{6}\left(1 + \frac{D_r}{D_p}\right)\sigma_b^0 t_p^2 \tag{A.11}$$

The displacements of the plate are then given by Eqs. (A12) and (A13)

$$u_b(0) = \frac{t_p}{2}\left(w_p'(0) - w_r'(0)\right) = -\frac{t_p t_a}{2E_a}\sigma_a'(0) = \kappa_b\frac{t_p t_a}{2E_a}B \tag{A.12}$$

$$u_m(0) = t_a(u_p(0) - u_r(0)) + u_b(0) = \frac{t_a}{G_a}A + \kappa_b\frac{t_p t_a}{2E_a}B \tag{A.13}$$

At this point, the spring compliance coefficients may easily be found, and are given by Eqs. (9)–(12).

References

Albat, A.M., Romilly, D.P., 1999. A direct linear-elastic analysis of double-symmetric bonded joints and reinforcements. Composites Science and Technology 59, 1127–1137.

ANSYS Release 9.0., 2004. ANSYS Inc. Canonsburg, Pennsylvania, USA.

Arendt, C., Sun, C.T., 1994. Bending effects of asymmetric adhesively bonded composite repairs on cracked aluminum panels. In: Proceedings of the FAA/NASA International Symposium on Advanced Structural integrity for Airframe Durability and Damage Tolerance, NASA conference publication 3274, Part1, pp. 33–48.

Baker, A.A., 1993. Repair efficiency in fatigue-cracked aluminum components reinforced with boron/epoxy patches. Fatigue and Fracture of Engineering Materials and Structures 16 (7), 753–765.

Clark, R.J., Romilly, D.P., 2001. Fatigue damage prediction for bonded composite repairs applied to metallic aircraft structures. SAE Journal of Aerospace, paper# 2001-01-26.

Clark, R.J., Romilly, D.P., 2002. Experimental study of a bonded composite repair. 2002 CSME Forum, May 21–24, Kingston, Ontario, Canada.

Clark R.J., Romilly D.P., 2003. Non-linear bending study of hybrid aluminum and boron–epoxy bonded joints. CANCOM 2003, Ottawa, Ontario, Canada.

Clark, R.J., Romilly, D.P., submitted for publication. Reinforced cracks in transversally isotropic generalized pane strain plates. Theoretical and Applied Fracture Mechanics.

Clark R.J., Romilly D.P., submitted for publication. Bending of transversally isotropic generalized plane strain plates with reinforced cracks. International Journal of Fracture.

Duong, C.N., Wang, C.H., 2004. On the characterization of fatigue crack growth in a plate with a single-sided repair. Transactions of the ASME 126, 192–198.

Goland, M., Reissner, E., 1949. The stresses in cemented joints. Journal of Applied Mechanics – Transactions of the ASME 66, A17–A27.

Jones, R., 1983. Neutral axis offset effects due to crack patching. Composite Structures 1, 163–174.

Jones, R., Callinan, R.J., Aggarwal, K.C., 1983. Analysis of bonded repairs to damaged fibre composite structures. Engineering Fracture Mechanics 17 (1), 37–46.

Jones, R., Chiu, W.K., Smith, R., 1995. Airworthiness of composite repairs: failure mechanisms. Engineering Failure Analysis 2 (2), 117–128.

Joseph, P.F., Erdogan, F., 1987. Plates and shells containing a surface crack under general loading conditions. NASA contractor report 178232, NASA Langley Research Center.

Joseph, P.F., Erdogan, F., 1989. Surface crack problems in plates. International Journal of Fracture 41, 105–131.

Kotousov, A., Wang, C.H., 2002. Fundamental solutions for the generalized plane strain theory. International Journal of Engineering Science 40, 1775–1790.

Papanikos, P., Tserpes, K.I., Labeas, G., Pantelakis, Sp., 2005. Progressive damage modelling of bonded composite repairs. Theoretical and Applied Fracture Mechanics 43, 189–198.

Ratwani, M.M., 1979. Cracked adhesively bonded laminated structures. AIAA Journal 17 (9), 988–994.

Romilly D.P., Clark R.J., 2005. Damage tolerance analysis and testing of unbalanced bonded composite repairs for aluminum airframes. SAE 05-AMT-41.

Rose, L.R.F., 1981. An application of the inclusion analogy for bonded reinforcements. International Journal of Solids and Structures 17, 827–838.

Rose, L.R.F., 1982. A cracked plate repaired by bonded reinforcements. International Journal of Fracture 18 (2), 135–144.

Rose, L.R.F., 1988. Theoretical Analysis of crack patching. In: Baker, A.A., Jones, R., (eds.), Bonded Repair of Aircraft Structures. Martinus Nijhoff, pp. 77–105.

Rose, L.R.F., Wang, C.H., 2002. Analytical methods for designing composite repairs. In: Baker, A.A., Rose, L.R.F., Jones, R. (Eds.), Advances in the Bonded Composite Repair of Metallic Aircraft Structure. Elsevier, Chapter 7.

Schubbe, J.J., Mall, S.S., 1999. Modelling of cracked thick metallic structure with bonded composite patch repair using three-layer technique. Composite Structures 45 (3), 185–193.

Volkersen, O., 1938. Rivet strength distribution in tensile-stressed rivet joints with constant cross-section. Luftfahrforschung 15 (1), 41–47.

Wang, C.H., Rose, L.R.F., 1997. On the design of bonded patches for one-sided repair. In: Proceedings of the 11th International Conference on Composite materials, Gold Coast, Australia, vol. 5, pp. 347–356.

Wang, C.H., Rose, L.R.F., 1998. Bonded repair of cracks under mixed-mode loading. International Journal of Solids and Structures 35 (21), 2749–2773.

Wang, C.H., Rose, L.R.F., 1999. A crack-bridging model for bonded plates subjected to tension and bending. International Journal of Solids and Structures 36, 1985–2014.

Wang, C.H., Callinan, R.J., Rose, L.R.F., 1998. Analysis of out-of-plane bending of a one-sided repair. International Journal of Solids and Structures 35 (14), 1653–1675.

Wen, P.H., Aliabadi, M.H., Young, A., 2002. Boundary element analysis of flat cracked panels with adhesively bonded patches. Engineering Fracture Mechanics 69, 2129–2147.